Band gap bowing and electron localization of $Ga_xIn_{1-x}N$

Byounghak Lee* and Lin-Wang Wang

Computational Research Division, Lawrence Berkeley National Laboratory, Berkeley, California 94720

Abstract

The band gap bowing and the electron localization of $Ga_xIn_{1-x}N$ are calculated using both local density approximation and screened-exchange local density functional (sX-LDA) method. The calculated sX-LDA band gaps are in much better agreement with the experimentally observed values with errors of -0.26 and 0.09 eV for bulk GaN and InN, respectively, compared with the local density approximation (LDA) estimations, whose band gap errors are 1.33 and 0.81 eV, correspondingly. In contrast to the gap itself, the band gap bowing parameter is found to be very similar in sX-LDA and LDA. We identify the localization of hole states in $Ga_xIn_{1-x}N$ alloys along In-N-In chain. The predicted localization is stronger in sX-LDA.

PACS numbers: 71.15.Mb, 71.20.-b, 71.23.-k, 71.23.An, 71.55.Eq

*Electronic address: bhlee@lbl.gov

The semiconductors based on group-III nitrides are important for photoelectronic applications, such as ultraviolet[1]/blue[2]/green [3] light-emitting diodes and lasers. By making alloy compounds, the frequency of the emitted light can be harnessed in a wide range. For example, the band gap of InN and GaN is $\approx$ 0.8 and 3.5 eV, respectively, and the alloy compounds $Ga_xIn_{1-x}N$ have band gaps spanning nearly the entire solar energy spectrum. [4, 5] The electronic structure and the carrier distribution of disordered alloys is valuable information for designing materials with desirable properties for various applications.

The band gap dependence of the III-nitride semiconductor alloys has been theoretical studied primarily using empirical pseudopotential method,[6] the local density approximation (LDA) of the density functional theory.[7, 8] While LDA is reliable in calculating the atomic relaxation and formation energies of the semiconductor alloys, it is well known that the band gaps calculated from these methods are underestimated due to its intrinsic errors in describing the excited states. The LDA calculated band gap of pure III-nitrides are significantly smaller than the experiments.[9, 10] The more accurate many-body GW method, on the other hand, has not been used for alloy calculations because of its high computational cost. There is no clear understanding of whether the LDA band gap errors in pure bulk crystals will cause significant errors in the band gap behavior in the alloy, especially for quantities such as the bowing parameters.

In addition to the band gap, the carrier localization in the III-nitride alloys is also an important issue. In $Ga_xIn_{1-x}N$ alloys, for example, there is large amount of defects. These defects of high concentration usually quench the photoluminescence and reduce the carrier concentration. The blue laser, on the other hand, is achieved in high efficiency with small In concentration. It has been speculated that the high efficiency of $Ga_xIn_{1-x}N$ -based emitting devices could be due to a strong hole state localization.[2] The first principle calculations can shed light on this important property of the material.

Our approach in this paper is to study the electronic structures of the alloys using improved density functional theory. The screened-exchange local density functional (sX-LDA) method has been successful in many simple semiconductors, such as II-VI, III-V, and IV-IV alloys, correcting the band gap error in the LDA method.[11, 12] The sX-LDA improves the LDA band gap similarly to that of many-body GW calculations and also yields the ground state structure as good as LDA. Although more expensive than LDA, sX-LDA is still cost effective enough to be used for alloy calculations. We study $Ga_xIn_{1-x}N$ alloys in zinc-blende

(ZB) structure and focus on the band gap bowing and the electron wavefunction localization. Previously, we have used the similar approach to study $Ga_xAl_{1-x}N$ alloy.[13] In those systems, the Ga and Al atoms are similar and, as a result, the bowing parameter is very small and the localization due to alloying is weak. On the contrary, $Ga_xIn_{1-x}N$ provides a more interesting example with larger bowing parameter and stronger carrier localization.

We carried out the calculations using a plane-wave basis with Troullier-Martins norm-conserving pseudopotentials.[14] We performed the LDA calculations with the Ga $3d$ and In $4d$ electrons in the core with their effects on valence electrons included within the nonlinear core correction of Louie, Froyen, and Cohen.[15] We found that inclusion of these semi-core electrons in the valence electrons reduces the band gap by ~ 0.3 and 0.2 eV for bulk ZB GaN and InN, respectively, within the LDA method. For the sX-LDA calculations, inclusion of the semi-core electrons in the valence electrons causes a significant error in the pseudopotential calculations. This is in part because the exchange integrals between the semi-core wavefunctions and the valence wavefunctions are distorted by the use of the pseudo-wavefunctions instead of the original all-electron wavefunctions. Thus, additional terms are needed to correct this error. Here, for consistency, we calculated both LDA and sX-LDA with the semi-core electrons in the core. For III-nitrides, the valence band maximum state is strongly localized near N atoms and, as a result, the valence band spin-orbit splitting is small; e.g., 11 meV for GaN.[5] Subsequently, the spin-orbit coupling was not included in our calculations.

In Fig. 1, we show the electronic structure of bulk zinc-blende GaN and InN calculated from LDA and sX-LDA. In these pure alloy calculations, we used 19 special k-points in an irreducible wedge for the integration over the Brillouin zone. The kinetic energy cutoff in all calculations (including the alloys bellow) is 70 Ryd. In experiments, GaN and InN crystallize in wurtzite (WZ) structure under ambient conditions. In the present work we used ZB structure of these materials for computational simplicity. The electronic structure of ZB and WZ structures are similar and closely related. According to previous studies,[16] the wurtzite Γ point band gap is close to the zinc-blende Γ point band gap. We show the band gap of GaN and InN in ZB and WZ crystal structure in Table. I. The experimental direct band gap of WZ GaN scatters between 3.39-3.5 eV.[17, 18] While the sX-LDA result, 3.20 eV, agrees well with the experiments, the LDA result underestimates the gap by ~ 40 %. Also notice that the band gap difference between the ZB and the WZ structure is ≈ 0.2

eV both in experiments and sX-LDA. For InN the correction of sX-LDA is more pronounced. The recently experimentally measured band gap for WZ structure is 0.8 eV.[4] The sX-LDA result for WZ InN is 0.89 eV, which is in the same quality as in the many-body GW method. The LDA band gap, on the other hand, is negative and predicts a qualitatively incorrect metallic state. Another effect of sX-LDA on the band structures of both GaN and AlN is the increase of the valence band width by ~ 2 eV, which has been observed in other bulk semiconductors.[11]

To model the disordered zinc-blende $Ga_xIn_{1-x}N$ alloy with Ga molar fraction $0 < x < 1$, we employed the special quasi-random structures (SQSs). [20] SQSs are finite model systems constructed to mimic the radial correlation functions of an infinite random structure. They have been extensively used to study the electronic structures of alloys. We considered two classes of model systems of SQS8 and SQS16. In SQS8 the cell consists of n In, m Ga, and 8 N atoms with $n + m = 8$. In SQS16 the cell contains twice the number of atoms in SQS8. For each model system, the lattice constant was inferred from experimental lattice constant using Vegard's law.[21] The equilibrium atom positions were obtained by minimizing the total energy within LDA. A total of 16 k-point were used to integrate over SQS Brillouin zone for SQS8. Table II shows that the band gap difference between SQS8 and SQS16 is less than 0.1 eV for all alloy compounds. Further increase of SQS cell size does not change

TABLE I: Band gap of GaN and InN in zinc-blende and wurtzite crystal structures. Energy is in eV.

	LDA	sX-LDA	Experiment
GaN (ZB)	1.97	3.04	3.3[a]
GaN (WZ)	2.11	3.20	3.39[b], 3.5[c]
InN (ZB)	-0.22	0.76	
InN (WZ)	-0.014	0.89	0.8[d]

[a]Reference[19]

[b]Reference[17]

[c]Reference[18]

[d]Reference[4]

the band gap, indicating SQS16 is already large enough. We used SQS8 in our following calculations with confidence of band gap error of 0.1 eV.

We now study the band gap dependence of $Ga_xIn_{1-x}N$ on Ga molar fraction, x. We show the band energy difference between the valence band maximum (VBM) and the conduction band minimum (CBM) in the upper panel of Fig. 2. Both InN and GaN have direct band gap at Γ point and the position of the fundamental band gap does not change when they are mixed to form alloys. In spite of the large band difference between LDA and sX-LDA method, their bowing parameters are very similar. Through the whole compositional range, the difference between the LDA and sX-LDA band gap is almost a constant, ~ 1 eV. The quadratic fitting of the band gap to the formula

$$E_{Ga_xIn_{1-x}N} = xE_{GaN} + (1-x)E_{InN} - x(1-x)b \quad (1)$$

leads to 1.48 (LDA) and 1.67 eV (sX-LDA) as the bowing parameter b. Here E_A is the band gap of materials A. The experimentally observed bowing parameter is 1.4 eV.[4] Taking into account the pseudopotential error and the difference between the ZB and WZ structures, we can conclude that both LDA and sX-LDA bowing parameters agree well with experiments. This similarity of LDA and sX-LDA in the bowing parameter has also been observed in our previous study.[13] Our results confirm the applicability of the LDA to the band gap bowing parameter in III-nitride systems. This is an important finding because many of previous studies on semiconductor alloys have been conducted using LDA method.

To further understand the band gap bowing, we show the energy levels of VBM and CBM states separately in the lower panel of Fig. 2. We have aligned the top of valence band of the LDA and sX-LDA results for InN. We found that the band alignments of different Ga molar fraction x are different for LDA and sX-LDA. Although the difference between the LDA and sX-LDA band gap is almost a constant for all x, that is no longer true for CBM and

TABLE II: The LDA band gap dependence on SQS cell size. Band gaps (eV) of ZB $Ga_xIn_{1-x}N$ with Ga molar fraction x are listed.

x	0	0.25	0.5	0.75	1.0
SQS8	-0.22	0.08	0.52	1.09	1.97
SQS16	-0.22	0.12	0.50	1.17	1.97

VBM energies separately. The situation is different in $Ga_xAl_{1-x}N$, where the VBM curves for LDA and sX-LDA are almost the same.

To study the carrier localization in $Ga_xIn_{1-x}N$, we first look into the self-consistent charge density changes from LDA to sX-LDA. Fig. 3 shows the radially averaged charge density centered around each constituent atoms in GaN and InN. Electrons are highly localized on N atoms and the bond charge is displaced toward N atoms from its nominal bond center position. We observe that, within the same method, the charge density around N atoms does not significantly change from GaN to InN. Because the erroneous self-interaction in LDA is partially corrected in sX-LDA, the sX-LDA produces a larger charge transfer towards the N atoms. Similar effect has been observed in other semiconductors, such as Si and GaAs, where sX-LDA produces a larger bond charge.

The photoluminescence of semiconductor materials is related to the VBM and CBM states rather than the total electron density. As discussed before, the possible hole state localization is important in $Ga_xIn_{1-x}N$ alloys. In Fig. 4 we show the sX-LDA result of the VBM charge density of $Ga_{0.5}In_{0.5}N$. The VBM wavefunction is localized around N atoms. Comparing the VBM density of LDA and sX-LDA, we found that the localization is stronger in sX-LDA. One of the features of Fig. 4 (b) is that the VBM state has larger wavefunction amplitude along In-N-In chains. This particular chain localization of cubic $Ga_xIn_{1-x}N$ VBM wavefunction has previously been observed in a semi-empirical pseudopotential model study. [6] Both LDA and sX-LDA calculation confirm this important finding. In order to measure the localization more quantitatively, we have calculated the participation ratio, $V\int|\psi(\mathbf{r})|^4 d\mathbf{r}$, which is 1 for constant wavefunctions and larger than 1 for any spatially varying wavefunctions. Here V is the volume over which the wavefunction is normalized. The stronger the localization, the larger the participation ratio. We show the participation ratio in Table III. The participation ratio for $Ga_xIn_{1-x}N$ alloys is much larger than that of the pure bulk materials. This confirms

TABLE III: The participation ratio dependence of $Ga_xIn_{1-x}N$ on Ga molar fraction x.

x	0	0.25	0.5	0.75	1.0
LDA	11.08	14.24	14.01	14.60	11.00
sX-LDA	12.17	14.55	14.87	15.87	11.15

that the VBM state is localized upon alloying. Comparing LDA and sX-LDA result, we found that the hole state localization is stronger in sX-LDA. In the whole range of x, the participation ratio of sX-LDA is larger than that of LDA. It is now well-known that sX-LDA correctly predicts stronger bonding structures compared with LDA.[22, 23] The enhanced bonding structure normally accompanies increased localization of wavefunctions. In $Ga_xIn_{1-x}N$, however, the charge transfer turns out to be more complicated than just an increase of the bonding strength. Fig. 4 (c) reveals that the localization in In-N-In chain is enhanced in sX-LDA results while the hole state in Ga-N-Ga chain is depleted.

In conclusion, we calculated the electronic structure of $Ga_xIn_{1-x}N$ and found that sX-LDA prediction of band gaps agrees well with the experiments. The band gap correction of sX-LDA is from both CBM and VBM in contrast to our earlier study of $Ga_xAl_{1-x}N$, where the band gap correction is mostly from CBM. In spite of large band gap correction of sX-LDA, the bowing parameter is similar in sX-LDA and LDA. We also identified the hole state localization along the In-N-In chain in $Ga_xIn_{1-x}N$ alloy in both sX-LDA and LDA. The sX-LDA prediction of this localization is stronger than the LDA prediction. This strong localization may explain the high efficiency of the light emitting devices based on $Ga_xIn_{1-x}N$.

This work was supported by U.S. Department of Energy under contract No. DE-AC03-76SF00098 and the calculations were done using resources of NERSC at Lawrence Berkeley National Lab.

---

[1] S. Nakamura, Semicond. Sci. Technol. **14**, R27 (1999).

[2] S. Nakamura, *The Blue Laser Diode GaN based Light Emitters and Lasers* (Springer, Berlin, 1997).

[3] S. Nakamura, M. Senoh, N. Iwasa, S. Nagahama, T. Yamada, and T. Makai, Japan. J. Appl. Phys. **34**, L1332 (1995).

[4] J. Wu, W. Walukiewicz, K. M. Yu, J. W. A. III, E. E. Haller, H. Lu, J. Schaff, Y. Saito, and Y. Nanishi, Appl. Phys. Lett. **80**, 3967 (2002).

[5] O. Madelung, M. Schulz, and H. Weiss, eds., *Intrinsic Properties of Group IV Elements and III-V, II-VI, and I-VII Compounds*, vol. 22 Pt. a of *Landolt-Bornstein, New Series* (Springer,

Berlin, 1987).

[6] L.-W. Wang, Phys. Rev. B **63**, 245107 (2001).

[7] E. A. Albanesi, W. R. L. Lambrecht, and B. Segall, Phys. Rev. B **48**, 17841 (1993).

[8] A. F. Wright and J. S. Nelson, Appl. Phys. Lett. **66**, 3051 (1995).

[9] A. F. Wright and J. S. Nelson, Phys. Rev. B **51**, 7866 (1995).

[10] C. Stampfl and C. G. V. de Walle, Phys. Rev. B **59**, 5521 (1999).

[11] A. Seidl, A. Görling, P. Vogl, J. A. Majewski, and M. Levy, Phys. Rev. B **53**, 3764 (1996).

[12] C. B. Geller, W. Wolf, S. Picozzi, A. Continenza, R. Asahi, W. Mannstadt, A. J. Freeman, and E. Wimmer, Appl. Phys. Lett. **79**, 368 (2001).

[13] B. Lee and L.-W. Wang, Phys. Rev. B **73**, 153309 (2006).

[14] N. Troullier and J. Martins, Solid State Commun. **74**, 613 (1990).

[15] S. G. Louie, S. Froyen, and M. L. Cohen, Phys. Rev. B **26**, 1738 (1982).

[16] C.-Y. Yeh, S.-H. Wei, and A. Zunger, Phys. Rev. B **50**, 2715 (1994).

[17] S. Strite and H. Morkoç, J. Vac. Sci. Technol. B **10**, 1237 (1992).

[18] B. Monemar, Phys. Rev. B **10**, 676 (1974).

[19] K. Lawniczak-Jablonska, T. Suski, I. Gorczyca, N. E. Christensen, K. E. Attenkofer, E. M. G. R. C. C. Perera, J. H. Underwood, D. L. Ederer, and Z. L. Weber, Phys. Rev. B **61**, 16623 (2000).

[20] S.-H. Wei, L. G. Ferreira, J. E. Bernard, and A. Zunger, Phys. Rev. B **42**, 9622 (1990).

[21] L. Vegard, Z. Phys. **5**, 17 (1921).

[22] R. Asahi, W. Mannstadt, and A. J. Freeman, Phys. Rev. B **59**, 7486 (1999).

[23] B. Lee and L.-W. Wang, Appl. Phys. Lett. **87**, 262509 (2005).

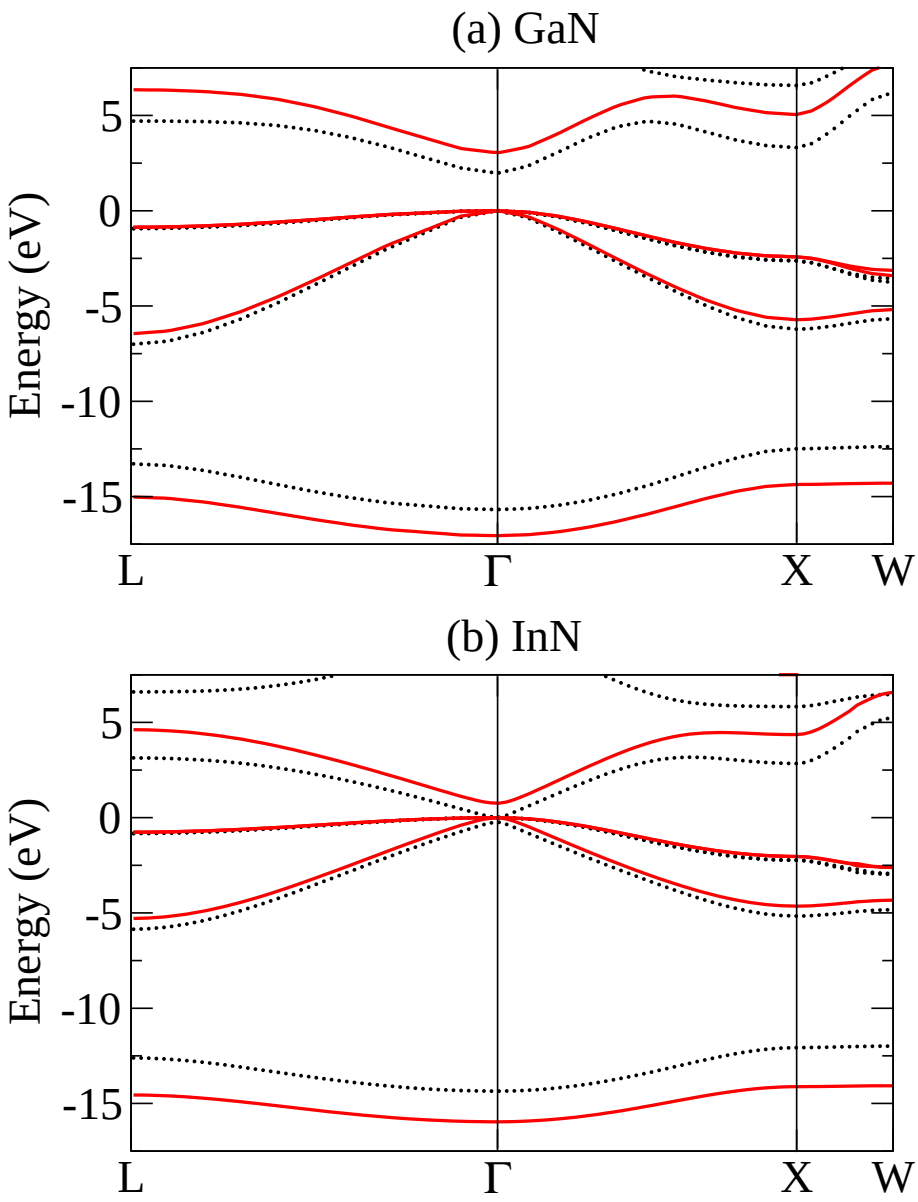

FIG. 1: The electronic band structure of zinc-blende nitrides, (a) GaN and (b) InN. The solid lines are the sX-LDA results and the dots are the LDA results. The bands are adjusted so that VBM energy is located at zero. Experimental lattice constant $a = 4.5$ Å for GaN and $a = 4.98$ Å for InN were used.

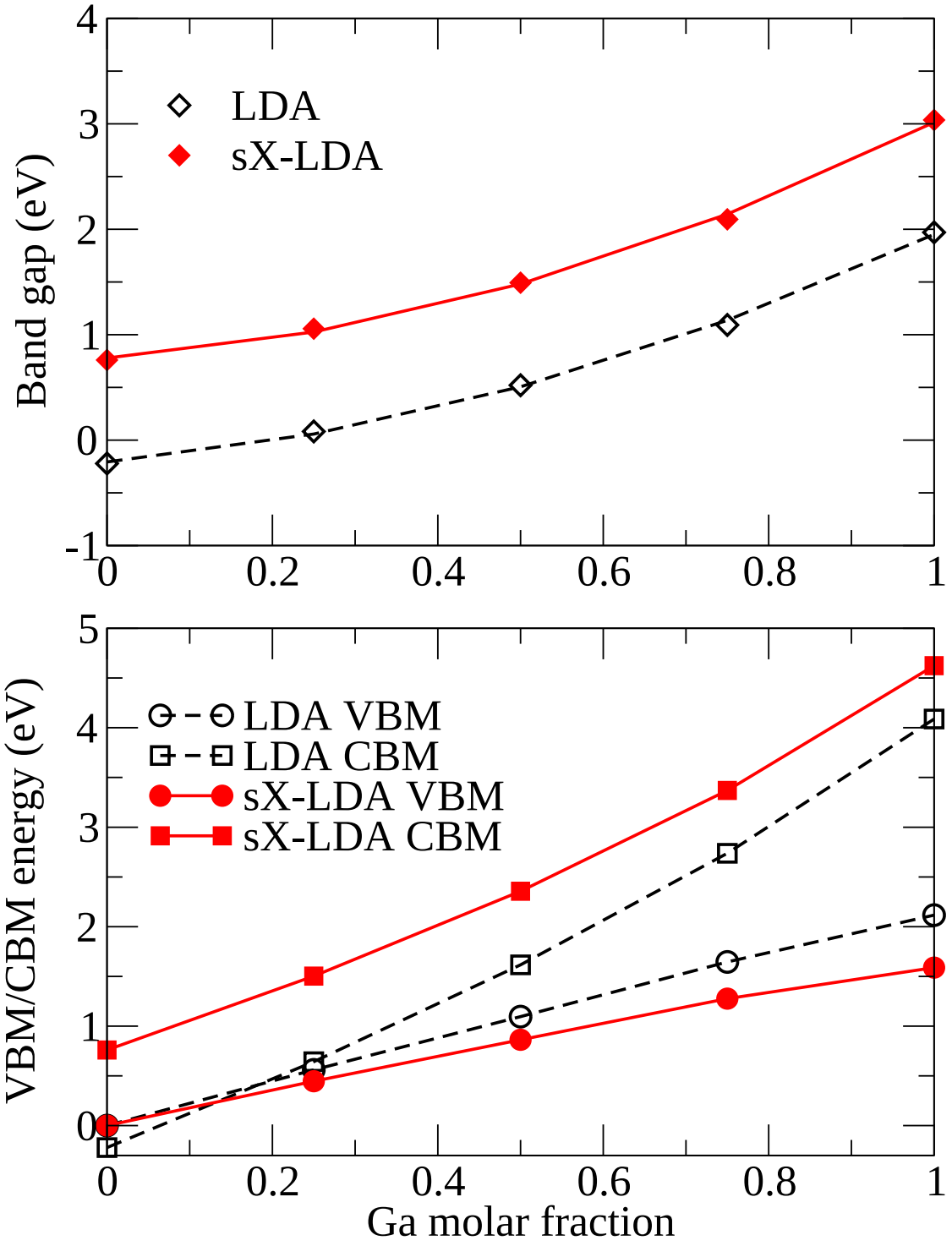

FIG. 2: Ga molar fraction x dependence. Upper panel: The band gap as a function of Ga molar fraction. The solid (dashed) line is the quadratic fitting of the numerical data in sX-LDA (LDA) calculations. Lower panel: VBM (circle) and CBM (square) eigenvalues as a function of Ga molar fraction. The filled and empty symbols are from sX-LDA and LDA, respectively.

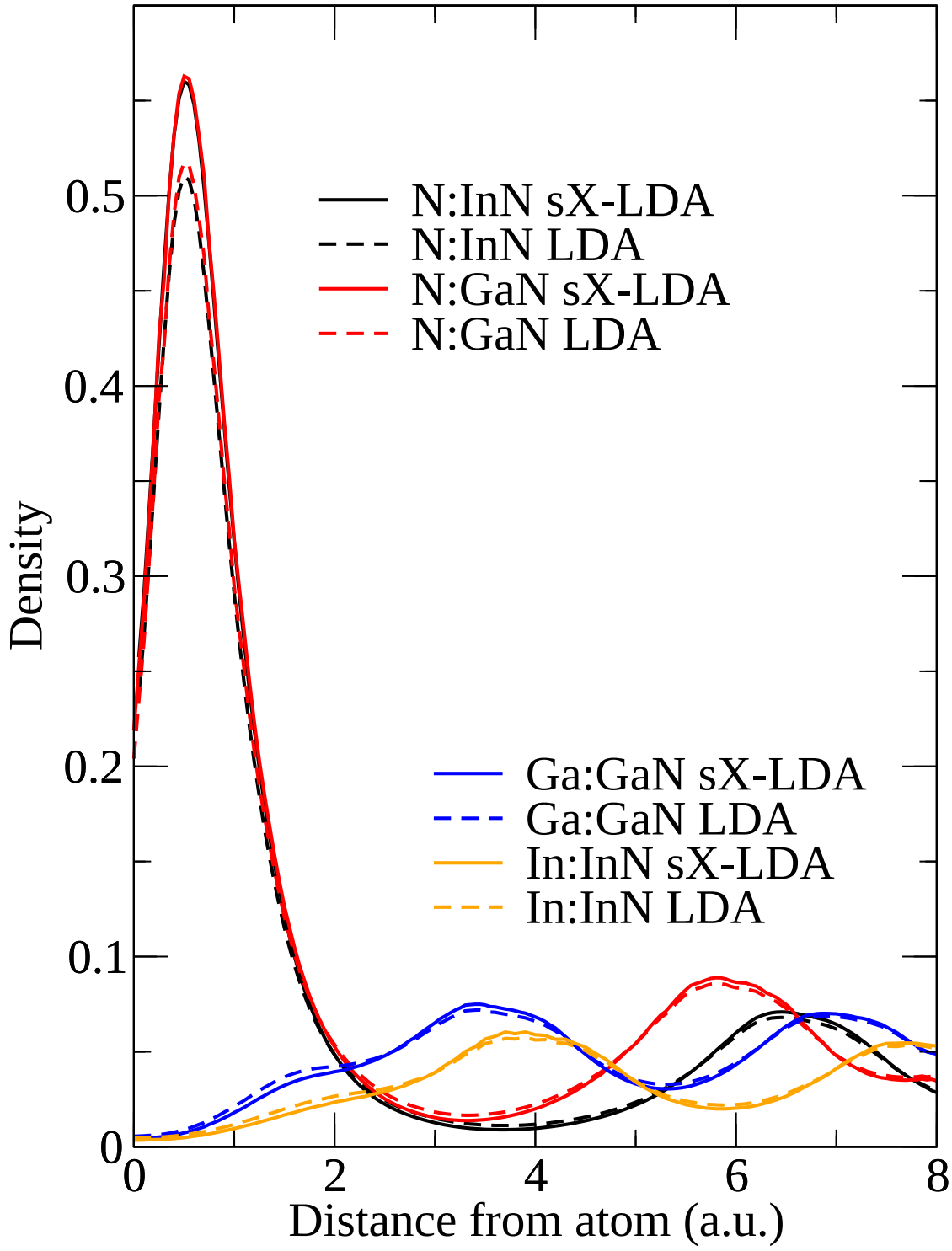

FIG. 3: Radially averaged charge density from the constituent atoms. Solid lines are from sX-LDA and dashed lines are from LDA.

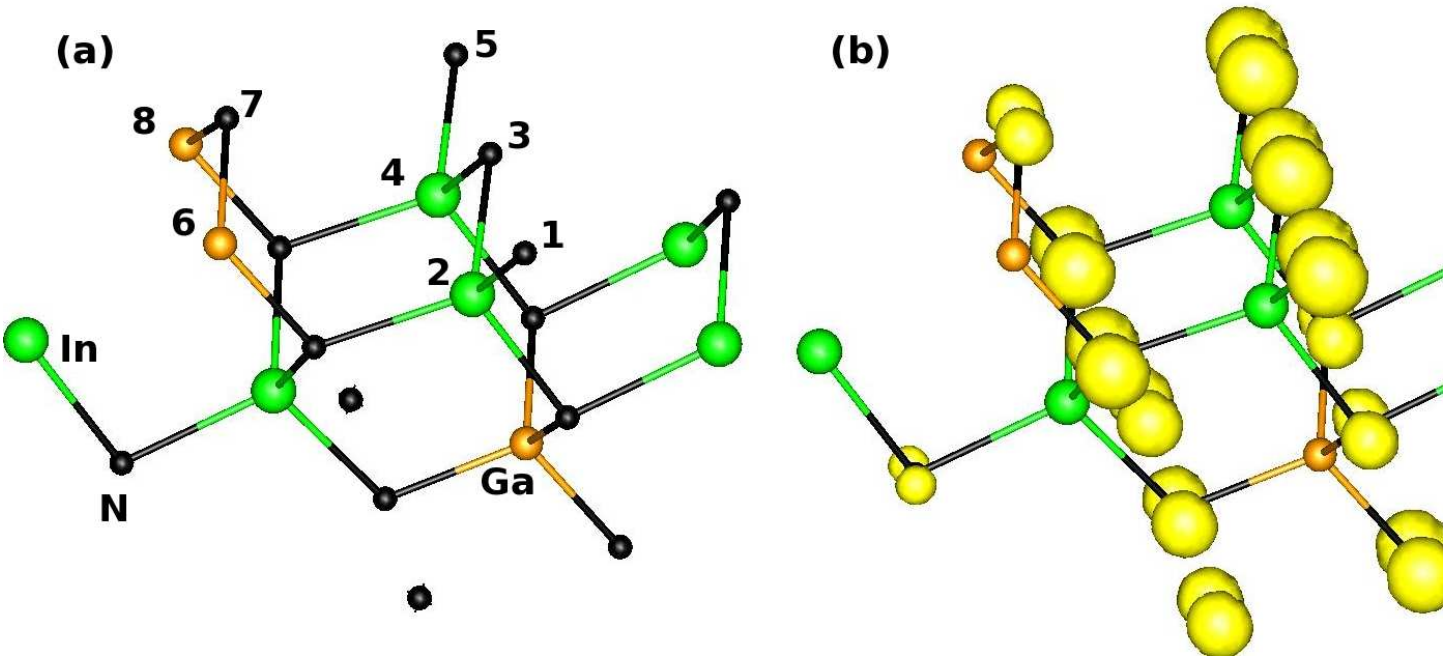

FIG. 4: VBM charge density of $Ga_{0.5}In_{0.5}N$ (a) Partial view of SQS supercell geometry. The large green, medium orange, small black spheres correspond to In, Ga, and N, respectively. The chain of 1-2-3-4-5 is a typical In-N-In chain. The chain of 6-7-8 is a prototype Ga-N-Ga chain. (b) The yellow bubbles are the equal VBM wavefunction amplitude surfaces calculated from sX-LDA, $|\psi^{\text{sX-LDA}}_{\text{VBM}}(\mathbf{r})|^2$. (c) The VBM wavefunction amplitude difference between sX-LDA and LDA; $\Delta n_{\text{VBM}}(\mathbf{r}) = |\psi^{\text{sX-LDA}}_{\text{VBM}}(\mathbf{r})|^2 - |\psi^{\text{LDA}}_{\text{VBM}}(\mathbf{r})|^2$. The red bubbles are positive constant Δn_{VBM} surfaces and the blue bubbles are negative constant Δn_{VBM} surfaces.